Available online at www.sciencedirect.com

Manufacturing Letters

Manufacturing Letters 33 (2022) 249–258

50th SME North American Manufacturing Research Conference (NAMRC 50, 2022)

Residual stress and material flow prediction in Friction Stir Welding of Gr2 Titanium T-joints

Davide Campanella, Gianluca Buffa*, Daniele Lamia and Livan Fratini

University of Palermo, viale delle Scienze, 90128 Palermo, Italy

* Corresponding author. Tel.: +39-09123861869; fax: +39-09123861869. *E-mail address:* gianluca.buffa@unipa.it

Abstract

Friction Stir Welding is nowadays an established technique successfully used by many industries. However, most of the research and, consequently, most of the applications regard aluminum alloys and butt joints. T-joints are of high interest for different industrial sectors as aeronautical, aerospace, naval and ground transportation, for which joint integrity and low residual stress are extremely important. In this study, an experimental and numerical approach is proposed with the aim to study the peculiarities of the residual stress distribution and material flow occurring in FSW of CP-Ti T-joints. Experiments were carried out to assess the feasibility of the process and to acquire the temperature data needed for the validation of a specifically set-up numerical model. Peculiar numerical strategies have been defined in order to calculate the residual stress with affordable CPU time and to highlight the bonding surface between the skin and the stringer. Main findings include a longitudinal residual stress profile different from the one usually found for butt joints. The reasons for this behavior were explained through a deep investigation on the temperature distribution in space and evolution in time. Finally, the bonding surface between skin and stringer was highlighted together with the possibility of flow defects in the fillet area.

Keywords: Friction Stir Welding; Titanium alloys; T-joints, FEM model; residual stress.

1. Introduction

Friction Stir Welding (FSW) is a promising solid-state joining technique invented and patented in 1991 by The Welding Institute. The process consists of 3 main phases: plunging, dwelling, and feeding of a rotating tool along the welding line. The tool has a specially designed geometry and during the process keeps a proper tilt angle that contributes to the welding success. Due to the tool stirring, the friction and the plastic deformation causes a temperature rising that activates, with the right process parameters, the solid-state joining mechanism. In other words, the joining is achieved without the problems associated with the melting transformation. The complex material flow caused by the tool action of stirring and feeding, affects the welding quality, an aspect extensively investigates for butt joints, especially as the process was initially proposed [1].

Important applications of FSW can be seen in the aeronautical field. In fact it can be used to weld materials like aluminum alloys of 2XXX and 7XXX series [2] that aren't weldable with traditional fusion welding, as a replacement of the riveting [3]. Different studies have shown how the FSWed joints show enhanced characteristics of corrosion resistance [4,5] and fatigue properties [6,7] compared to conventional welding techniques like TIG and MIG, replacing them in different applications.

Until now, most of the research has concentrated on two joint configurations: butt and lap. Nevertheless, the T-joint design (made of skin and stringer sheets) is widely utilized in a variety of industrial applications, including but not limited to the aeronautical/aerospace area [8]: *Shipbuilding industry* for

producing ship hulk, mast, etc.; *Railways industry* for joining wagon components and floorboards; *Aviation industries* for the reinforcement of fuselage; *Automobile applications* for the welding of car bodies, fuel tanks, back supports, bicycle as well as motorcycles frames, and *Construction industry* for connecting bridges, pipelines and window frames.

One of the main reasons for the use of FSW for the production of T-joints is the possibility to produce the so called skin and stringer structures with just one welding pass against the two usually needed with more conventional processes i.e. Laser Welding, TIG, etc [9]. Additionally, especially in the aero-structure field, the use of other techniques as riveting would result in an increase of the plane weight while adding the manufacturing procedure of the pre hole, with detrimental stress concentration effects [10].

As far as the production of titanium alloys T joints by FSW is regarded, two possible approaches can be found in literature: (i) the stationary shoulder friction stir welding (SSFSW) based approach, for which two passes are made on the T fillet corners to create the joint; (ii) the FSW "transparency" approach, for which only one pass on the top surface of the skin is needed. Edwards and Ramulu found that the performance of corner joints in fatigue could be compared to butt joint data when a geometrically based stress concentration factor is applied [11]. Su et. al. adapted the transparency approach utilizing three sheets thus having the tool passed twice [12].

Due to the complex material flow, the significant number of process parameters and the high cost of the raw material, numerical simulation can be considered as an indispensable tool for the process design. However, the simulation of the FSW process requires the setup of a highly non-linear numerical model due to the complex process mechanics. Indeed, the stirring action and the feeding advancing of the tool generates large displacement and distortion in the region around the pin, with consequent heat generation due to friction and deformation work. This peculiar process mechanics allows the generation of a solid-state weld with reduced Heat Affected Zone (HAZ) and a Recrystallized Zone (RZ) close to weld seam. Because of the process complexity, several approaches are suitable for the numerical model of the process. From a literature analysis, it does not appear to exist still today a dominant numerical method to simulate the process. Colegrove P.A. [13] was among the first to examine the effect of slip in 2-dimensional flow around the pin using a 2D CFD approach on FLUENT. The aim was to optimize a 2-dimensional pin profile minimizing the traverse force while maintaining the rotational torque. More recently, Isa et al. [14] presented a review on the "Recent research progress in friction stir welding of aluminum and copper dissimilar joint", in which two main approaches are described: Computational Fluid Dynamics (CFD) and Coupled Eulerian-Lagrangian (CEL) Computational Solid Mechanics (CSM). The authors highlighted how the coupled frictional heat generation, the formation and development of plastic flow region, and the three-dimensional heat and material flow can be investigated by both approaches. Naumov et al. [15] investigated the effect of tapered hexagonal tool probe profile on the macrostructure, mechanical performance, and material flow of AA2024−T4 joined by friction stir welding. In order to achieve this goal, the authors used a CFD model to determine the temperature and effective strain rate distribution during the process. Arora et al. [16] reported the computed strains and strain rates during FSW of AA2524 from a three-dimensional coupled viscoplastic flow and heat transfer model. To obtain this, the strain rates were integrated along a streamline to estimate the accumulated strains experienced by the material. Zhang et al. [17] established a solid mechanics-based thermo-mechanical Eulerian model to study the torque, the power, and the heat generations from pin side surface, pin tip surface, and shoulder contact surface in different rotating speeds in FSW. The results were compared to the experimental data and the ones obtained with an ALE model. Meyghani B. [18] employed a modified friction model to investigate the relationship between the shear stress, the pressure and the relative velocity using a Combined Eulerian CSM model to a FE Model in Abaqus CAE. Veljić et al. [19] used ALE method to simulate the heat generation during the plunge stage in FSW. Assidi et al. [20] investigated a friction model to better reproduce the process, tuning the numerical ALE model, utilizing the software Forge, with experimental results. Jain [21] simulated the process using a Lagrangian implicit FE Model to predict forces, spindle torque, temperature and plastic strain. Xiao et al. [22] developed an explicit coupled method of FEM and the meshless particle method to simulate the temperature distributions during FSW of Al 6061-T6 plates. As a solid state technique, the heat input is limited with respect to both conventional and innovative fusion-based processes, hence the buildup of residual stress is limited as well. However, the determination of the residual stress distribution is a key aspect to effective joint design. Different analytical and experimental research studies have been conducted on residual stress measurement in FSW. Bussu and Irving studied the effects of weld residual stress and heat affected zone on the fatigue propagation of cracks parallel and orthogonal to the weld direction in friction stir welded (FSW) 2024-T351 joints. The authors found that the weld residual stress was mechanically relieved and the effects on crack propagation were observed. [23]. Feng et al. proposed an integrated thermal-metallurgical-mechanical model to provide insights on the formation of the residual stress and the changes in microstructure and mechanical properties of AI6061-T6 friction stir welds. [24]. Sun et al. proposed a study of the residual stresses generated in stationary shoulder friction stir welds (SSFSWs) produced in a typical high strength aluminum alloy (AA7010). The authors showed how SSFSW, as compared to conventional FSW, produced narrower and more uniform weld nugget and heat affected zones profile through the plate thickness [25].

As far as numerical models for FSW of Ti alloys are regarded, only a quite limited number of papers can be found in literature. Some of the authors [26] presented a FEM model able to predict the phase transformations taking place during FSW of Ti6Al4V titanium alloy butt joints. In particular, the entire process was modeled, from the tool plunge to the final in air-cool down of the joint, by means of a model that is implicit, Lagrangian, thermo-mechanically coupled with visco-plastic material characterization. Recently, a time-dependent, three-dimensional, thermomechanical model of the FSW process was developed in order to understand the temperature profiles of various engineering materials such as steel, aluminium alloy and titanium alloy was studied by Sarikavak, Y. [27]. In the paper, the theoretical predictions and the experimental results showed that the maximum temperature gradients on the y- and z-axes were located at the outside diameter of the shoulder radius or at the center of the weld line according to the boundary conditions applied in the welding process.

To the authors best knowledge, no paper dealing with the numerical o experimental determination of the residual stress distribution in T-joints produced by FSW "in transparency" can be found in literature. Recently, Sun et al [28] proposed a study focused on the determination of the residual stress field in AAA7050 aluminum alloy T joints welded using a stationary shoulder with the fillet-corner technique. They found high tensile residual stress close to the edge of the pin.

The present paper presents the results of an experimental and numerical study aimed at the determination of the residual stress distribution and material flow in FSW of Ti grade2 T-joints. A dedicated clamping fixture was designed and, in order to generate proper heat input, two different tools have been tested to weld in "transparency" skin and stringer structures. The joints metallurgical and micro-mechanical properties have been acquired to analyze the joint produced under three different process conditions. Finally, a FEM model was set up and validated against experimental measurements in order to understand the process mechanics and predict the thermal and the residual stresses fields.

Nomenclature

FSW	Friction Stir Welding
SSFSW	Stationary Shoulder FSW
CLTE	Coefficient of Linear Thermal Expansion
HAZ	Heat Affected Zone
RZ	Recrystallized Zone
FEM	Finite Element Method
OM	Optical Microscope
SZ	Stir Zone
UHAZ	Upper Heat Affected Zone
LHAZ	Lower Heat Affected Zone
RS	Retreating Side
AS	Advanced Side

2. Experimental Process, modelling and validation

2.1. Experimental setup

For the tests, commercially pure Titanium Grade 2 sheets were used (the mechanical properties are shown in Table 1).

Table 1. Main mechanical properties of Ti grade 2 at room temperature.

Work material	Ti grade 2
Ultimate tensile strength [MPa]	485
Yield stress [MPa]	275
Modulus of elasticity [GPa]	110
Hardness [HV 5]	180
CLTE [1/°C]	9.1E-6

The tests were carried out on an ESAB LEGIO 3ST using a tilt angle (θ) of 2.5° and a tool plunge of 2.8 mm. In order to ensure the same plunge along the weld, a force control on the stirring head was set on the machine. Both the skin and stringer sheets, 2 mm thick, were reduced into rectangular specimens.

The experimental fixture utilized is depicted in Fig. 1. Steel plates polished on the grinding machine were utilized to ensure uniform pressure distribution on the specimens. After the stringer was secured between the vertical walls, the skin was positioned and clamped above it. Screw grains were employed to maintain pressure on the skin and prevent distortion during the process. Due of titanium's susceptibility to oxygen, the experiments were conducted under argon flux. (Fig. 1b).

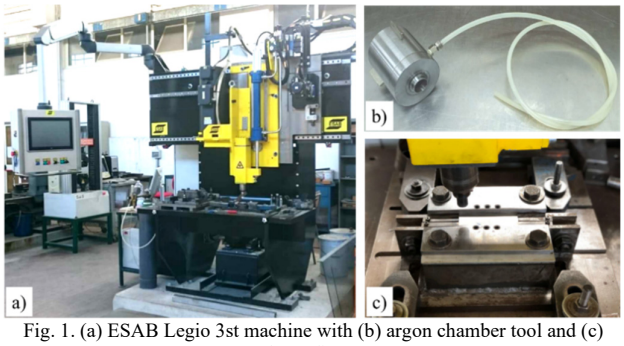

Fig. 1. (a) ESAB Legio 3st machine with (b) argon chamber tool and (c) Clamp fixture.

Two different pin tool temperature probes, one with double shoulder (Fig. 2a) and one with conventional conical pin (Fig. 2b) were tested to determine proper heat input. The tools were made in W-Re alloy characterized by a melting point of 3050 °C and a recrystallization temperature close to 1900 °C. Fig. 2c shows the geometrical parameters used for the final T-joint, which were inspired by genuine aeronautical and aerospace applications.

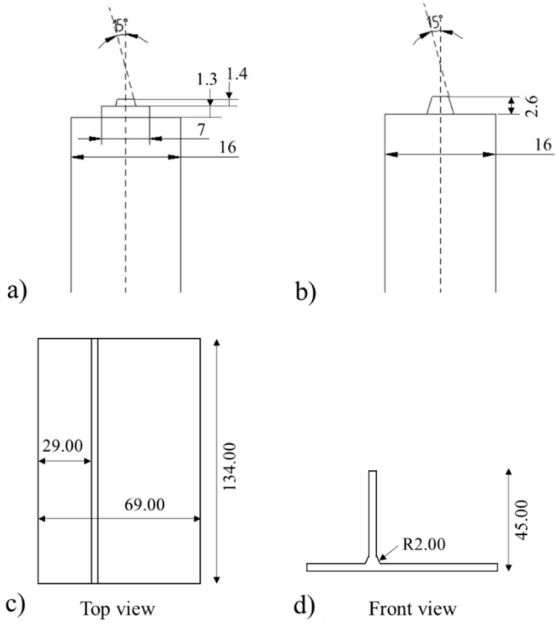

Fig. 2. Dimensions in millimeters for tools (a) with double shoulder, (b) without double shoulder and (c-d) for the final T-joint

In terms of process parameters, tool rotation was kept constant while varying feed rate was considered, as shown in table 3.

Table 3. Process parameters used

Feed rate [mm/min]	20	40	80
Rotational speed [rpm]		400	

Each test was repeated three times, and specimens were cross-sectioned perpendicular to the welding direction from each joint. The three welds were cross sectioned and examined using the Optical Microscope (OM) to evaluate the microstructure to assess the joint quality. Micrographs were also used to assess the occurrence of flow problems. To obtain such results, the specimens were hot mounted, polished, and then etched with Keller reagent before being viewed by an OM. A thermocouple K-type was inserted in the skin at 10 mm from the welding center at half weld seam length to examine the process and fine-tune the numerical simulation.

2.2. Numerical Model setup

Using the commercial software DEFORM-3D™, a thermo-mechanically coupled simulation with a Lagrangian formulation was set up. For the mechanical analysis, a rigid-viscoplastic material model was used, described in detail in [29]. To avoid numerical instabilities of a deformable-deformable contact, the two sheets to welded were modeled as a single block i.e. the two parts joined as a single geometry. The validity of this assumption has already been proved for butt and lap joint configuration [29]. Fig. 3 shows the meshed tool and the single block.

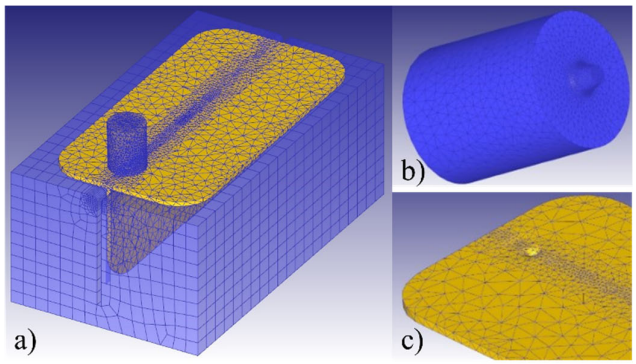

Fig. 3. (a) The FEM model for FSW process during the plunge phase: mesh of (b) the tool and (c) the workpiece

The sheet blank, 2 mm thick, was meshed with about 45000 tetrahedral elements. Because of the large gradients of the calculated variables, it was necessary to introduce a finer discretization along the welding line. Additionally, a re-meshing referring volume was identified all along the tool feed movement. In this area, each tetrahedral element had maximum single edge of about 0.3 mm; in this way, about five elements were placed along the sheet thickness. For the material assigned to this part, i.e. Titanium Type 2, the following values of thermal conductivity and thermal capacity, taken from DEFORM's material library, were used: k = 12 $N/(s\,°C)$ and c = 3 $N/(mm^2\,°C)$. No variation of k and c with temperature was taken into account. This assumption makes the thermal problem linear, speeding up the numerical solution at each time increment. Both the tool and the fixation plate, considered as a rigid body, were meshed for the thermal analysis, with respectively about 20000 tetrahedral 7500 hexahedral elements each. The material properties for both rigid parts were taken from DEFORM's material library, especially the DIN-C45 was assigned to the fixation plate. For the contact heat exchange coefficient, a constant value of 11 $[N/(s\,mm\,°C)]$ was utilized. Through a specially built subroutine, an interface penalty constant equal to 1E10 was applied to penalize the penetration velocity of the sheet nodes through the tool master surface. This prevented parts from folding, particularly in the contact area between the tool pin and the workpiece, where the material "closes" behind the tool, lowering the possibility of an unexpected simulation stop owing to convergence failure. Based on previous analysis made by some of the authors [30] a constant shear friction factor of 0.6 was used for the tool-sheet interface. A constant convection coefficient h = 0.02 $[N/(s\,mm\,°C)]$ was used to take in to account the heat exchange between the top surface of the skin and the environment at the constant temperature of 20 °C. The process can be divided in plunging and feeding phase; respectively a time step of 0.01 $s/step$ and 0.004 $s/step$ was used due to the different deformation condition. To evaluate the residual stress distribution in the workpiece at the end of the process, a special approach developed by some of the authors [31] was used.

Fig. 4 illustrates a flow chart of the FEM model utilized to obtain the residual stress from the elasto-viscoplastic model using temperature distribution interpolatated from the rigid-viscoplastic model.

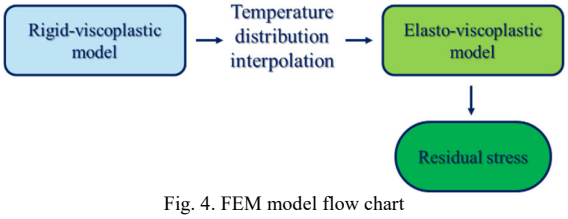

Fig. 4. FEM model flow chart

2.3. Model fine tuning and validation

As the residual stresses mainly depend on the thermal histories experienced by the workpiece, the model validation was carried out against experimentally measured temperatures. The "node tracking" option of the software DEFORM-3D™ was utilized, highlighting, for a node placed to 10 mm from the welding line, the temperature history. The reference transverse section was taken after ~60 mm of weld length, when the process has already entered a steady state and the obtained data are free from transient effects. The comparison between numerically calculated and experimentally measured temperatures for the three different case studies is shown in Fig. 5.

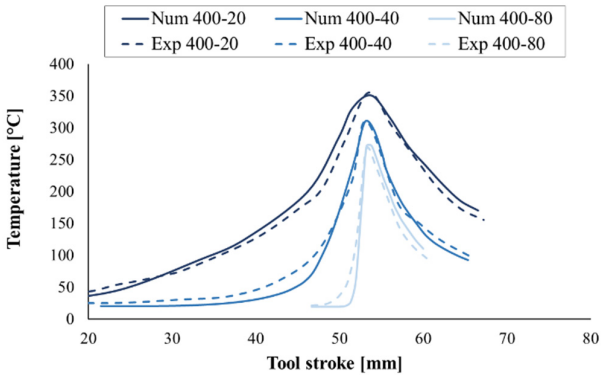

Fig. 5. experimental and numerical temperatures graph plot using single shoulder tool

In coherence with the experimental results, it can be seen that the temperature peak value decreases with increasing feed rate. Also, the time during which a given point experience high temperature increases with decreasing tool feed rate because of the higher heat input.

3. Results

3.1. Visual inspection

Based on existing literature [32], a double shoulder tool was used (Fig. 6a). Using the parameters 400 rpm - 40 mm/min, it was possible to generate a homogeneous weld although characterized by an excessive specific heat input both on the skin and on the stringer, as visible from the "burnished" areas close to the weld seam (Fig. 6a). In addition, by varying the feed rate, i.e. 20 mm/min and 80 mm/min, surface defects such as large voids and tearing, respectively, occurred.

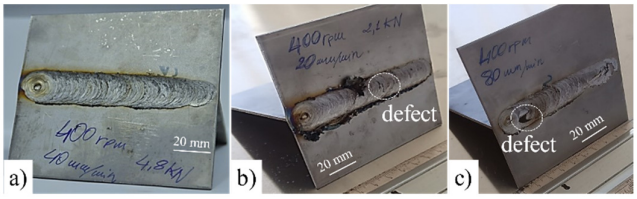

Fig.6. experimental test using double shoulder tool for 400 rpm and (a) 40 mm/min (b) 20 mm/min and (c) 80 mm/min case studies

The authors therefore resorted to a modification of the tool geometry (Fig.2b). With this modification, better results were obtained in different respects: a more uniform weld seam was noted; it was possible to obtain sound joints with a wider process window. Fig. 7 shows the results of the tests carried out with fixed tool rotation equal to 400 rpm and feed rate varying from 20 to 40 and finally 80 mm/min.

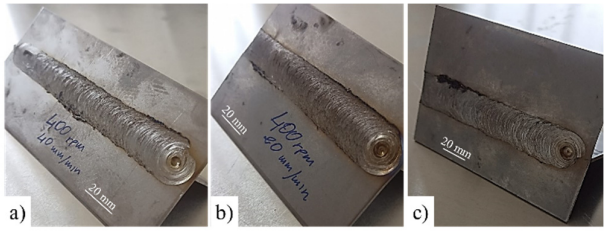

Fig. 7. experimental test using single shoulder tool for 400 rpm and (a) 40 mm/min (b) 20 mm/min and (c) 80 mm/min case studies

3.2 Mechanical and microstructure characterization

No internal defects were observed in the joints studied. In Fig. 8, the morphological analysis for the representative specimen characterized by 400 rpm and 40 mm/min is shown. The microstructure of the three typical areas, i.e. Stir Zone (SZ), Upper Heat Affected Zone (UHAZ) and Lower Heat Affected Zone (LHAZ) is shown;

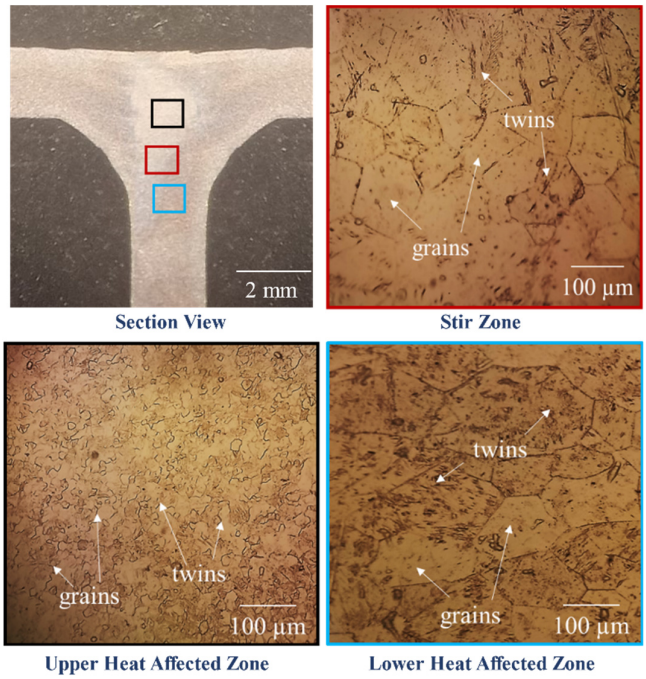

Fig. 8. Macro and micro observations for the experimental test carried out using single shoulder tool with 400 rpm - 40 mm/min

A SZ can be noticed in the skin center caused by the combination of high temperature and high strain.
In particular, the SZ exhibits equiaxed solid solution grains of size ~10 µm, while in the other zones ~100 µm grains are observed. The solid solution grains also exhibit banded structures similar to twins. Twinning is not typical of commercially pure titanium under ordinary conditions, but it occurs al low temperatures, e.g., in cold rolling [33], and /or at high strain rates. The twinning was earlier observed in FSWed joints on commercially pure titanium [34] and explained by the lack of slip system at a high strain rate.

3.3. Numerical results

3.3.1. Temperature distributions

As described in the previous paragraph, the first step of the developed procedure was the simulation of the welding process with a rigid-viscoplastic material model, based on the assumption that, due to the extremely large deformations occurring, elastic deformation can be neglected with no significant loss in the results accuracy. In this way the nodal temperatures and their evolution during the FSW process were calculated. Fig. 9 shows the temperature evolution on the top surface of the workpiece for process conditions characterized

by tool rotation of 400 rpm and tool feed rate of 40 mm/min. During the tool plunge, a temperature peak of about 715 °C is reached while a maximum level of about 924 °C is found once the process reached its steady state. It is important noting that a different shape of the temperature "comet" is observed with respect of FSW of butt joints. Instead of an ellipse-shaped comet [35], a hump can be noticed in the thermal field due to the peculiar T-Joint geometry as the heat transferred from the skin to the stringer causes a faster temperature decrease in the zone around the welding line. Furthermore, an asymmetrical behavior on the temperature field can be observed in the two sides of the welding line due to the asymmetrical geometry of the part (see again Fig. 2).

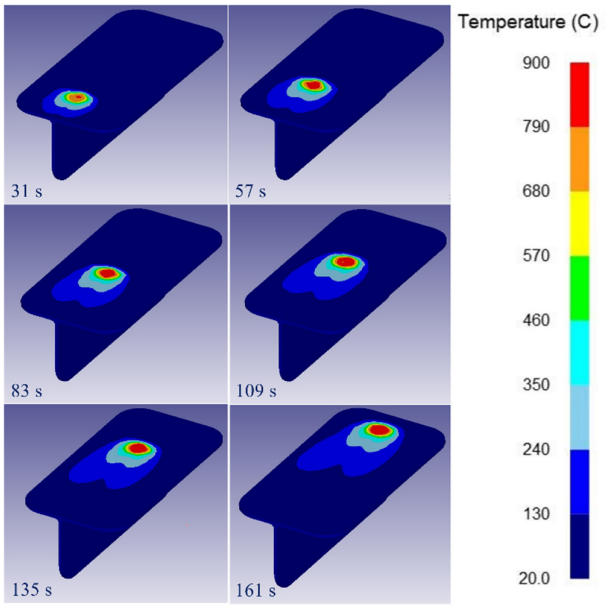

Fig. 9. Workpiece temperature evolution during the welding process simulation — 400 rpm and 40 mm/min case study.

To study the residual stress build-up, the temperature measured along a transverse line at mid length of the weld seam is shown in Fig. 10 as a function of time. The plot in Figure 9a hence represents a surface function of the process time and of the distance from the welding line. In particular, Fig. 10b shows how the maximum temperature reached by each point does not occur simultaneously, due to heat transfer from the center of the weld to the edges. In Fig. 10c it can be noticed how the asymmetric geometry affects the temperature peak on the transverse, line as previously mentioned. Fig. 10d shows how the nodal temperature has a higher temperature gradient when heating up - which is due to the tool work - than when cooling down - due to heat exchange by conduction and convection -. Analyzing the temperature behavior, the buildup of the residual stress can be understood: in the left part of the graph (from 35 s to 50 s), due to the high temperature increase, the inner elements will expand, compressing the sides element. In the right part (from 50 s to 80 s), the quick temperature decrease will induce the central elements to reduce their volume, generating localized tensile stresses around the weld seam.
Since this behavior is experienced by each section of the welding line, this will induce significant longitudinal stresses.

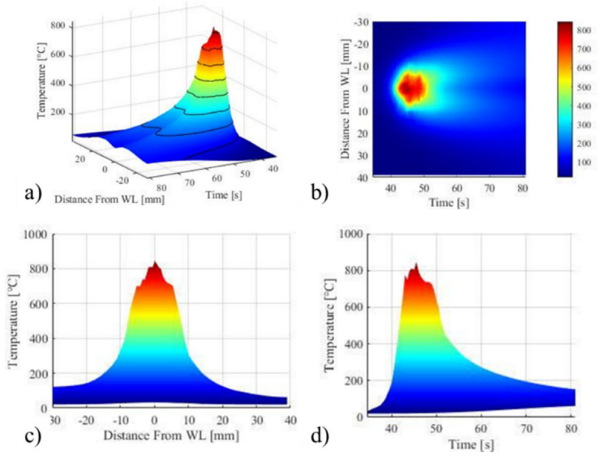

Fig. 10. Workpiece temperature map during the welding process simulation as a function of time and distance from the weld center — 400 rpm and 40 mm/min case study

The above-described temperature evolution can be better understood by observing the temperature distribution across a transverse section of the joint. Figure 10a shows the temperature when the tool has just passed by the considered section and the material has just closed behind it. The typical "bowl" shaped distribution observed in FSW of Ti alloys can be observed. Fig. 11b shows the temperature after 42.6 s, i.e. when the tool traveled about 23 mm. In this case an important difference with respect to what observed in butt and lap joints is noticed [35]: for the latter joint morphologies, the SZ is the hottest even after the tool passage, i.e. is the one that cools down for last; on the contrary, for the T joints, the central part of the SZ cools down rapidly to the presence of the skin. In this way, the hottest areas are the ones corresponding to the boundary between the pin action area and lateral part of the skin.

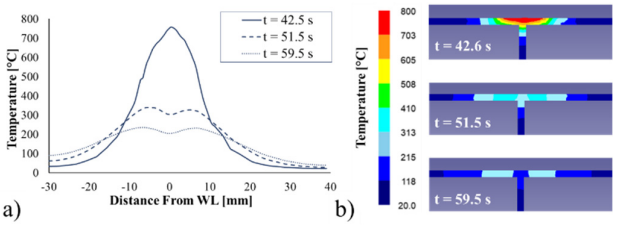

Fig. 11. Workpiece temperatures a) temperatures plot b) temperature distributions at datum time — 400 rpm and 40 mm/min case study

3.3.2. Residual stress distributions

In Fig. 12, the longitudinal residual stress distribution calculated for the case study characterized by 400 rpm - 40 mm/min is shown. It should be observed that the longitudinal stress distribution is the most interesting to investigate for FSW processes, as the largest residual stresses are expected parallel to the processing line, i.e. parallel to the tool trajectory as also demonstrated by Li et al. in their study [36].

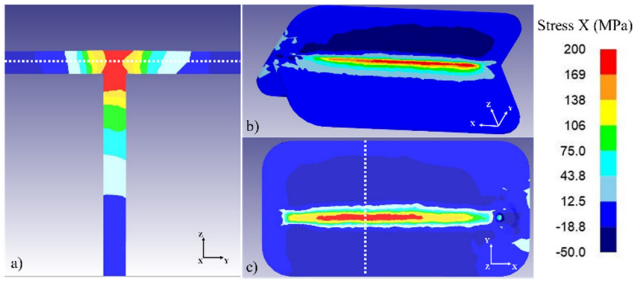

Fig. 12. Longitudinal residual stress distribution: (a) transversal section, (b) isometric view and (c) top view of the joint — 400 rpm and 40 mm/min case study.

As expected, when the process reaches its steady-state, tensile stress is found at the center of the joint all along the welding line and including the area interested by the tool action, while a compressive state can be observed at the periphery of the joint.

In Fig. 13 the residual longitudinal stresses calculated in a cross section along the line previously shown in Fig.11a is shown. A comparison can be made between the curves at different process parameters. Increasing the tool feed rate there will be a lower heat input reducing the temperature-time gradient, thus lowering the residual stresses generated in the joint. It is noted that, although this is the first time that residual stresses are reported for FSW of CP-Ti T-joints, the peak values calculated, ranging from about 170 MPa to about 220 MPa, are consistent with what found in literature for the FSW of Ti-6Al-4V butt joints, for which values in the range of 200-450 MPa are found [37].

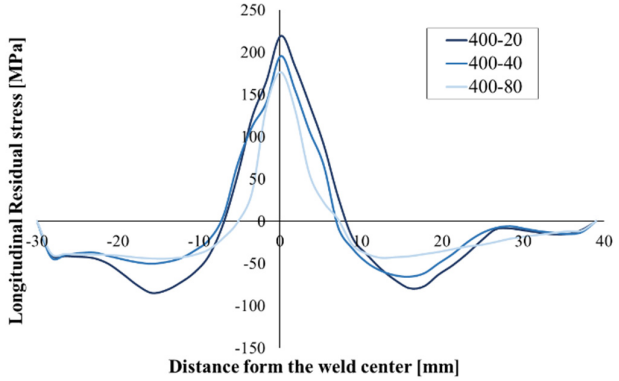

Fig. 13. Longitudinal residual stress distribution in a cross section along at mid height of the skin for the considered cases studies

Focusing on the shape of the residual stress distribution, a significant difference can be noted with respect to the one usually obtained for butt joints. As reported by many authors [37], an M-shape is obtained in the high tensile stress area close to the weld center, with peak values corresponding to the boundary between the SZ and the HAZ. Instead, for the T joints studied, a reverse V-shape was obtained. This can be explained looking at the temperature distributions and evolution in time shown in the previous paragraph. As well established, the buildup of longitudinal residual stress in FSW of butt joints is due to the rapid cooling of the SZ, the hottest area, which contracts generating tensile stress peaks in the already cooled zone corresponding to the shoulder edges (i.e. approximately the boundary between SZ and HAZ). On the other hand, in FSW of T-Joints, the more rapid cool down of the weld center, due to the conduction with the skin, results in hottest areas at the sides of the weld center. In these areas, contraction occurs generating a peak of residual stress at the center and the observed reverse V-shape. Based on these considerations, it is noted an inverted correspondence between temperature distribution and residual stress distribution in butt and T joints. In the former configuration, a reverse V-shape distribution is observed for temperature and an M-shape distribution is observed for the residual stress, while in the latter configuration the opposite is observed. Fig. 14 shows a schematic representation of the above-described different phenomena.

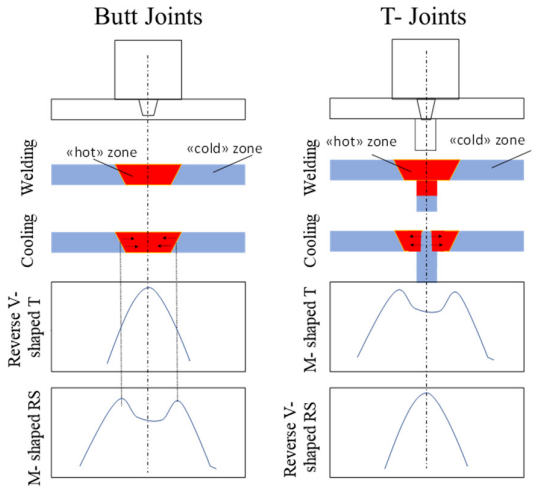

Fig. 14. Schematic representation of the different buildup of the residual stress in butt and T joints due to the temperature evolution

3.3.3. Material flow

In order to highlight the bonding surface and the occurring materials flow starting from a single block model, a numerical "trick" was used. The single block deformable object corresponding to the skin and the stringer was modeled with a biphasic material, in which each phase was assigned to a different "sheet" (i.e. skin or stringer) and has the same thermo-mechanical properties of the investigated CP-Ti. Fig. 15 shows as the separation line before, during and after tool pass moves down with higher displacement of the skin in the retreating side (R.S.) than the advanced side (A.S.) caused by the tilted tool action for the case study characterized by 400 rpm - 40 mm/min. In particular, the vertical component of the material flow, enhanced by the conical shape of the tool, results in a wavy profile of the bonding surface. However, both in the A.S. and in the R.S. the bonding between the two sheet edges occurs at about mid length of the fillet. Additionally, a close up of the fillet area is reported (Fig. 15d), from where the trace of the actual bonding surface, resulting from complex plastic flow generated during the process, can be observed. It is worth noting that the edges are a critical point for the joint strength as incomplete or incorrect bonding in these areas determines weak points from which fracture may propagate. Fig. 15e shows incomplete bonding obtained with 400 rpm and 160 mm/min. It can be seen that the "colder" process conditions determined poor fillet forging in the R.S and lack of bonding.

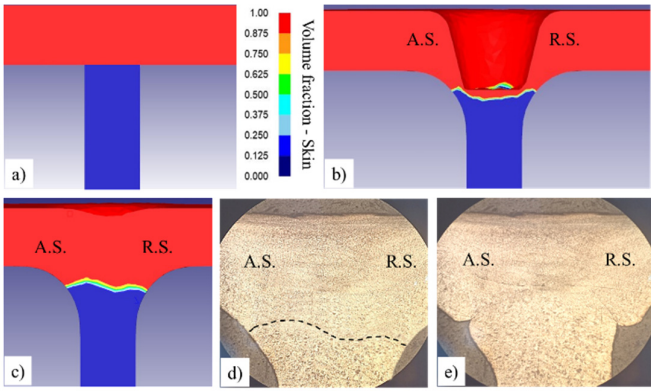

Fig. 15.Material flow in a cross section of the joint: (a) before, (b) during and (c) after the tool pass. Experimental micrographs of (d) the same joint cross section and (e) a joint obtained with too large feed rate.

4. Summary and Conclusions

In the paper, the results of an experimental and numerical study aimed at highlighting the residual stress distribution and the material flow in FSW of Grade 2 Titanium T-joints are reported. Experimental tests have been carried out to assess the feasibility of the process and to acquire the temperature data needed to validate a specifically set-up numerical model. The numerical model was then used to investigate the temperature and residual stress distributions as well as the occurring material flow which can lead to the formation of defects. From the obtained results the following conclusions can be drawn:

- ✓ Defect free T joints can be produced with a wider range of feed rate only if a conventional shoulder-pun tool is used. If a double shoulder tool is adopted, as the one successfully applied for similar joints in aluminum alloys, the excess of heat results in a very limited process window;
- ✓ The temperature distribution in the top surface of the skin shows a “hump” in the comet indicating that cool down is influenced by the presence of the stringer. For this reason, the last part of the cross section which cools down is not the weld center, as in butt joints, but rather the areas around the boundary between SZ and HAZ;
- ✓ The residual stress distribution is influenced by the process parameters, with increasing values observed with increasing heat input, i.e. with decreasing feed rate. Additionally, a reverse V shape distribution is found, differently from the M-shaped one usually found for butt joints. This different behavior is caused by the different temperature distribution highlighted;

The material flow analysis highlighted that the bonding surface is characterized by a wavy profile. At the external edges of the joint, the bonding surface trace corresponds to about half length of the fillet. This area is particularly critical as uncomplete bonding can generate crack propagation towards the weld center dramatically affecting the joint resistance.

References

[1] P.A. Colegrove, H.R. Shercliff, 3-Dimensional CFD modelling of flow round a threaded friction stir welding tool profile, Journal of Materials Processing Technology. 169 (2005) 320–327. https://doi.org/10.1016/j.jmatprotec.2005.03.015.

[2] P. Cavaliere, R. Nobile, F.W. Panella, A. Squillace, Mechanical and microstructural behaviour of 2024-7075 aluminium alloy sheets joined by friction stir welding, International Journal of Machine Tools and Manufacture. 46 (2006) 588–594. https://doi.org/10.1016/j.ijmachtools.2005.07.010.

[3] B.J. Dracup, W.J. Arbegast, Friction Stir Welding as a Rivet Replacement Technology, (n.d.).

[4] D.A. Wadeson, X. Zhou, G.E. Thompson, P. Skeldon, L.D. Oosterkamp, G. Scamans, Corrosion behaviour of friction stir welded AA7108 T79 aluminium alloy, Corrosion Science. 48 (2006) 887–897. https://doi.org/10.1016/j.corsci.2005.02.020.

[5] S. Maggiolino, C. Schmid, Corrosion resistance in FSW and in MIG welding techniques of AA6XXX, Journal of Materials Processing Technology. 197 (2008) 237–240. https://doi.org/10.1016/j.jmatprotec.2007.06.034.

[6] X. Wang, K. Wang, Y. Shen, K. Hu, Materials Comparison of fatigue property between friction stir and TIG welds, 2008.

[7] P.M.G.P. Moreira, M.A.V. de Figueiredo, P.M.S.T. de Castro, Fatigue behaviour of FSW and MIG weldments for two aluminium alloys, Theoretical and Applied Fracture Mechanics. 48 (2007) 169–177. https://doi.org/10.1016/j.tafmec.2007.06.001.

[8] K. Krasnowski, Experimental Study of FSW T-joints of EN-AW 6082-T6 and Their Behaviour Under Static Loads, Arabian Journal for Science and Engineering. 39 (2014) 9083–9092. https://doi.org/10.1007/s13369-014-1465-0.

[9] S.M.O. Tavares, P.C.M. Azevedo, B. Emílio, V. Richter-Trummer, M.A. v Figueiredo, P. Vilaça, P.M.S.T. de Castro, IMECE2008-67522 FRICTION STIR WELDING OF T-JOINTS IN DISSIMILAR ALUMINIUM ALLOYS, n.d. http://www.asme.org/about-asme/terms-of-use.

[10] G. Zhou, X.Q. Yang, L. Cui, Z.H. Zhang, X.D. Xu, Study on the microstructures and tensile behaviors of friction stir welded T-joints for AA6061-T4 alloys, Journal of Materials Engineering and Performance. 21 (2012) 2131–2139. https://doi.org/10.1007/s11665-012-0154-y.

[11] P. Edwards, M. Ramulu, Fatigue performance

of Friction Stir Welded titanium structural joints, International Journal of Fatigue. 70 (2015) 171–177. https://doi.org/10.1016/j.ijfatigue.2014.09.013.

[12] Y. Su, W. Li, F. Gao, A. Vairis, Effect of FSW process on anisotropic of titanium alloy T-joint, Materials and Manufacturing Processes. (2021). https://doi.org/10.1080/10426914.2021.1942911.

[13] Colegrove P.A., MODELLING AND DEVELOPMENT OF THE TRIVEX TM FRICTION STIR WELDING TOOL, 2004.

[14] M.S.M. Isa, K. Moghadasi, M.A. Ariffin, S. Raja, M.R. bin Muhamad, F. Yusof, M.F. Jamaludin, N. bin Yusoff, M.S. bin Ab Karim, Recent research progress in friction stir welding of aluminium and copper dissimilar joint: a review, Journal of Materials Research and Technology. 15 (2021) 2735–2780. https://doi.org/10.1016/j.jmrt.2021.09.037.

[15] A. Naumov, E. Rylkov, P. Polyakov, F. Isupov, A. Rudskoy, J.-N. Aoh, A. Popovich, O. Panchenko, Effect of Different Tool Probe Profiles on Material Flow of Al–Mg–Cu Alloy Joined by Friction Stir Welding, Materials. 14 (2021) 6296. https://doi.org/10.3390/ma14216296.

[16] A. Arora, Z. Zhang, A. De, T. DebRoy, Strains and strain rates during friction stir welding, Scripta Materialia. 61 (2009) 863–866. https://doi.org/10.1016/j.scriptamat.2009.07.015.

[17] Z. Zhang, H.W. Zhang, Solid mechanics-based Eulerian model of friction stir welding, International Journal of Advanced Manufacturing Technology. 72 (2014) 1647–1653. https://doi.org/10.1007/s00170-014-5789-4.

[18] B. Meyghani, A modified friction model and its application in finite-element analysis of friction stir welding process, Journal of Manufacturing Processes. 72 (2021) 29–47. https://doi.org/10.1016/j.jmapro.2021.10.008.

[19] D.M. Veljić, M.P. Rakin, M.M. Perović, B.I. Medjo, Z.J. Radaković, P.M. Todorović, M.N. Pavišić, Heat generation during plunge stage in friction stir welding, Thermal Science. 17 (2013) 489–496. https://doi.org/10.2298/TSCI120301205V.

[20] M. Assidi, L. Fourment, S. Guerdoux, T. Nelson, Friction model for friction stir welding process simulation: Calibrations from welding experiments, International Journal of Machine Tools and Manufacture. 50 (2010) 143–155. https://doi.org/10.1016/j.ijmachtools.2009.11.008.

[21] R. Jain, S.K. Pal, S.B. Singh, A study on the variation of forces and temperature in a friction stir welding process: A finite element approach, Journal of Manufacturing Processes. 23 (2016) 278–286. https://doi.org/10.1016/j.jmapro.2016.04.008.

[22] Y. Xiao, H. Wu, An Explicit Coupled Method of FEM and Meshless Particle Method for Simulating Transient Heat Transfer Process of Friction Stir Welding, Mathematical Problems in Engineering. 2020 (2020). https://doi.org/10.1155/2020/2574127.

[23] G. Bussu, P.E. Irving, The role of residual stress and heat affected zone properties on fatigue crack propagation in friction stir welded 2024-T351 aluminium joints, 2003. www.elsevier.com/locate/ijfatigue.

[24] Z. Feng, X.L. Wang, S.A. David, P.S. Sklad, Modelling of residual stresses and property distributions in friction stir welds of aluminium alloy 6061-T6, Science and Technology of Welding and Joining. 12 (2007) 348–356. https://doi.org/10.1179/174329307X197610.

[25] T. Sun, M.J. Roy, D. Strong, P.J. Withers, P.B. Prangnell, Comparison of residual stress distributions in conventional and stationary shoulder high-strength aluminum alloy friction stir welds, Journal of Materials Processing Technology. 242 (2017) 92–100. https://doi.org/10.1016/j.jmatprotec.2016.11.015.

[26] G. Buffa, A. Ducato, L. Fratini, FEM based prediction of phase transformations during Friction Stir Welding of Ti6Al4V titanium alloy, Materials Science and Engineering A. 581 (2013) 56–65. https://doi.org/10.1016/j.msea.2013.06.009.

[27] Y. Sarikavak, An advanced modelling to improve the prediction of thermal distribution in friction stir welding (FSW) for difficult to weld materials, Journal of the Brazilian Society of Mechanical Sciences and Engineering. 43 (2021). https://doi.org/10.1007/s40430-020-02735-2.

[28] T. Sun, M.J. Roy, D. Strong, C. Simpson, P.J. Withers, P.B. Prangnell, Weld zone and residual stress development in AA7050 stationary shoulder friction stir T-joint weld, Journal of Materials Processing Technology. 263 (2019) 256–265. https://doi.org/10.1016/j.jmatprotec.2018.08.022.

[29] G. Buffa, J. Hua, R. Shivpuri, L. Fratini, A continuum based fem model for friction stir welding - Model development, Materials Science and Engineering A. 419 (2006) 389–396. https://doi.org/10.1016/j.msea.2005.09.040.

[30] Fratini L., Beccari S., Buffa G., Friction stir welding fem model improvement through inverse thermal characterization, in: Transactions of the North American Manufacturing Research Institute of SME,

2005: pp. 259–266.
[31] G. Buffa, A. Ducato, L. Fratini, Numerical procedure for residual stresses prediction in friction stir welding, Finite Elements in Analysis and Design. 47 (2011) 470–476. https://doi.org/10.1016/j.finel.2010.12.018.
[32] D. Campanella, G. Buffa, A. Barcellona, L. Fratini, Friction stir welding of Ti6Al4V complex geometries for aeronautical applications: A feasibility study, in: Procedia Manufacturing, Elsevier B.V., 2020: pp. 93–97. https://doi.org/10.1016/j.promfg.2020.08.017.
[33] S. v. Zherebtsov, G.S. Dyakonov, G.A. Salishchev, A.A. Salem, S.L. Semiatin, The Influence of Grain Size on Twinning and Microstructure Refinement During Cold Rolling of Commercial-Purity Titanium, Metallurgical and Materials Transactions A: Physical Metallurgy and Materials Science. 47 (2016) 5101–5113. https://doi.org/10.1007/s11661-016-3679-0.
[34] W.B. Lee, C.Y. Lee, W.S. Chang, Y.M. Yeon, S.B. Jung, Microstructural investigation of friction stir welded pure titanium, Materials Letters. 59 (2005) 3315–3318. https://doi.org/10.1016/j.matlet.2005.05.064.
[35] Buffa G., Ducato A., Fratini L., Micari F., Advanced FEM modeling of friction stir welding of Ti6Al4V: Microstructural evolutions, in: Transactions of the North American Manufacturing Research Institution of SME, 2013: pp. 667–676.
[36] T. Li, Q.Y. Shi, H.K. Li, W. Wang, Z.P. Cai, Residual stresses of friction stir welded 2024-T4 joints, in: Materials Science Forum, Trans Tech Publications Ltd, 2008: pp. 263–266. https://doi.org/10.4028/www.scientific.net/msf.580-582.263.
[37] M. Meisnar, J.M. Bennett, D. Andrews, S. Dodds, R. Freeman, R. Bellarosa, J. Kelleher, A. Graham, A.F. Norman, T. Rohr, T. Ghidini, Advanced manufacturing of titanium propellant tanks for space applications part 2: a comparative study of residual stresses, CEAS Space Journal. (2021). https://doi.org/10.1007/s12567-021-00398-w.